Thermodynamics of bouncing grains

O. Devauchelle [*]
Université de Paris, Institut de Physique du Globe de Paris, 1 rue Jussieu, CNRS, 75238 Paris, France

P. Popović
Faculty of Physics, University of Belgrade, P.O. Box 44, 11001 Belgrade, Serbia

P. Szymczak
Institute of Theoretical Physics, Faculty of Physics, University of Warsaw, Pasteura 5, 02-093 Warsaw, Poland

A. Abramian
Sorbonne Université, CNRS, Institut Jean Le Rond d'Alembert, F-75005 Paris, France

A. Lazarus
Sorbonne Université, CNRS, Institut Jean Le Rond d'Alembert, F-75005 Paris, France and Massachusetts Institute of Technology, Department of Mathematics, Cambridge, Massachusetts 02139, USA

(Received 7 May 2026; accepted 15 July 2026; published 24 August 2026)

When a horizontal plate vibrates strongly enough, it causes small particles such as sand grains to continually bounce on it and, over time, to diffuse across its surface. This phenomenon is the cause of the well-known Chladni figure, which is drawn by a higher density of grains gathering along the nodal lines of a resonating elastic plate. Using a heterogeneous, nonresonating plate, we investigate experimentally this type of diffusion. We find that, for the most part, it is comparable to classical molecular diffusion. We can define a temperature for the bouncing grains, and the system then obeys the fluctuation-dissipation theorem. We also recover Maxwell-Boltzmann statistics at equilibrium, when temperature is uniform. However, when temperature varies across the vibrating plate, the microscopic details of the grains' dynamics affect their macroscopic behavior: Fick's law, for instance, no longer applies. Instead, our experiments support a new transport relation that was recently proposed to represent diffusion in Chladni's experiment. Finally, we propose an expression for the heat flux associated to the nonequilibrium steady state predicted by this new relation and test it against observations.

DOI: 10.1103/zlsc-w7m4

I. INTRODUCTION

The formation of the Chladni figure—the gathering of sand grains along the nodal lines of a vibrating plate [1]—has long been attributed to an average force, of ambiguous origin, that would deterministically drive the particles [2–4]. The tracking of individual grains over a vibrating membrane, however, suggests a simpler explanation: The grains are random walkers which gather where their diffusivity D is weak [5], as first suggested by Grabec [6].

Perhaps surprisingly, this simple phenomenon cannot be represented by Fick's law, which states that the average flux of particles is

$$\mathbf{j} = -D\nabla\rho, \tag{1}$$

where ρ is the average density of particles. In equilibrium, indeed, the Fickian flux must vanish, and the concentration is then uniform, regardless of any variation in diffusivity. This paradox was first noted by Büttiker [7] and Landauer [8] who suggested that Fick's law be replaced with

$$\mathbf{j} = -\nabla(D\rho), \tag{2}$$

under some conditions, which could be those of a rarefied gas [9–11]. Then, when the flux of particles vanishes, the density of particles must be inversely proportional to diffusivity:

$$\rho \propto \frac{1}{D}. \tag{3}$$

This relation is observed experimentally in Chladni figures [5]. Sand grains bouncing on a vibrated surface, therefore, can be seen as a macroscopic analog of the thought experiment introduced by Büttiker [7] and Landauer [8]—an analog in which, conveniently, the motion of individual particles can be experimentally tracked.

Hereafter, we call "statistical equilibrium" the steady state associated to Eq. (3), in reference to the absence of any particle flux ($\mathbf{j} = 0$), and in contrast with true thermodynamic equilibrium, for which the energy flux also needs to vanish. Büttiker [7] went beyond this statistical equilibrium. He remarked that, when combined with a suitable potential force, a periodic temperature field could sustain a constant current of

[*]Contact author: devauchelle@ipgp.fr

particles, thus driving a Brownian motor, now referred to as a "Büttiker-Landauer (BL) ratchet"—a nonequilibrium steady state that is *not* in statistical equilibrium ($\mathbf{j} \neq 0$). The analogy with the Chladni figure implied that a macroscopic version of the BL motor could be made with bouncing grains. In a companion paper, we present such an experimental realization, and show that it behaves essentially as predicted by Büttiker [7]: A constant, average current of particles emerges from the random bouncing of sand grains [12].

Over the years, the BL motor has attracted the attention of theoreticians, not only because the development of nanoscale devices makes its physical realization seem ever more accessible, but also because its thermodynamics is intriguing [13]. The main difficulty in assessing the motor's efficiency is to evaluate the leakage of heat along the temperature gradient. Benjamin and Kawai [14] addressed this issue both theoretically and with numerical molecular dynamics, but their conclusions remain to be experimentally tested—which is obviously challenging with molecular systems.

Here we use a bouncing-grain experiment to investigate the statistics and thermodynamics associated to Eq. (2). The setup is the same as in the companion paper [12], but hereafter we focus on the steady state associated to Eq. (2), wherein neither particle current nor external force complicates the picture. It is thus a simpler system than the BL motor, but it nonetheless features the heat flux that dominates the energy balance of the motor. On a more conceptual level, this heat flux also keeps the system away from thermodynamic equilibrium, even when the particle flux $\mathbf{j}$ vanishes, and thus directly relates to the departure from Boltzmann's statistics that the Chladni figure requires.

We first consider the trajectories of the bouncing grains, and check classical results from statistical physics, such as the Maxwell-Boltzmann distribution of velocities and the fluctuation-dissipation relation (Sec. II). We then justify the use of Eq. (2) to represent the diffusion of grains bouncing over a heterogeneous substrate (Sec. III), and finally measure the heat flux associated to the statistical equilibrium of bouncing grains by tracking their individual trajectories (Sec. IV).

II. BOUNCING GRAINS

A. Experimental setup

Inspired by the historical experiments of Chladni [1], and more recent versions of it [5,6], we devise a setup in which the vertical vibration of a plate causes irregular quartz grains to bounce erratically [Figs. 1(a) and 1(b)]. The grains thus roam across a horizontal disk (radius $R = 3.9$ cm), made of rigid PVC and bounded by a 2 cm-high PMMA wall which confines the grains over the disk. The surface of the disk is either simply painted green, and thus remains hard, or machine tooled with a milling machine to carve a 1 mm-deep groove into which vinyl polysiloxane (VPS), a soft elastomer, is molded (pink area in Fig. 2). This groove can cover the entire surface of the disk [Fig. 2(a)], be absent [Fig. 2(b)], or cover only a small rectangle [heterogeneous substrate, Fig. 2(c)]. This allows us to alter the bounciness of the substrate, and thus cause the grains to behave differently over different areas of

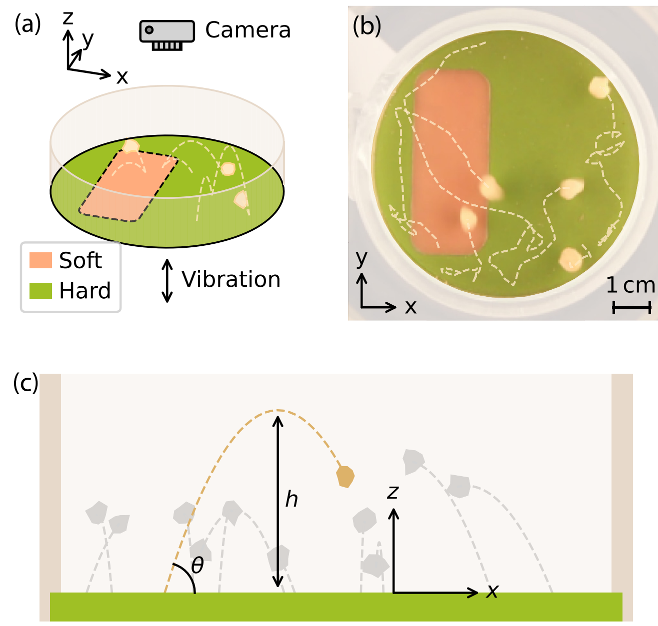

FIG. 1. (a) Experimental setup. The disk vibrates along the z axis. The setup can be tilted by a few degrees around the x axis. Quartz grains bounce randomly over a hard plastic surface (green, PVC), or a soft silicone polymer (pink, vinyl polysiloxane). (b) Still frame from an experimental movie (run C). Dashed white lines show the grains' trajectories during 1.5 s (75 frames). (c) Idealized representation of the bouncing grains. Their trajectory during a jump is a free fall (dashed lines).

the vibrating disk. To keep the grains from sticking on the elastomer, we cover all disks with Parafilm M.

The PVC disk is fixed on a vertical aluminum shaft, the motion of which is constrained by two translating positioners that can only move along an optical rail. The verticality of this translation device, and therefore the horizontality of the vibrating disk, can be adjusted manually with a three-axis rotation stage. A disposable plastic cup connects the lower end of the shaft to the membrane of a bass loudspeaker (8 Ω), which is driven by a function generator (Hameg HM8030-6) through a 40 W amplifier (Kemo M034N). The typical vibration frequency ν is between 30 and 40 Hz.

The particles we deposit on the vibrating plate are sand grains, mostly made of quartz, sieved into size classes (Tables I and II). For each experimental run, we introduce a small number of grains (five to ten) from a single class. The

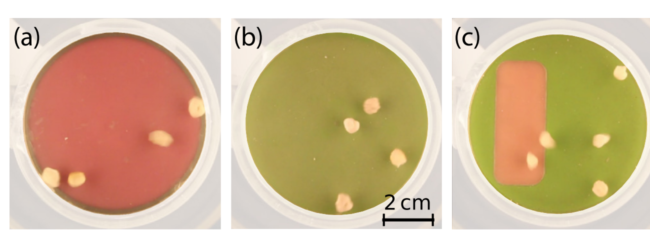

FIG. 2. The three substrates used in the experiment. (a) Soft elastomer (pink, VPS). (b) Hard plastic (green, PVC). (c) Heterogeneous substrate.

TABLE I. Experimental parameters for the first series of experiments. The substrate is heterogeneous [Fig. 2(c)]. The corresponding data are used in the companion paper [12]. The vibration amplitude, which is constant during each run, was not recorded for this series. Brackets indicate sieve size for d_s. Numbers in gray indicate difference between autocorrelation and dispersion for D, and standard deviation, computed over a series of movies, for v_{rms}.

Run	A	B	C	D	E	F	G	H
Frequency ν [Hz]	30.6	30.4	29.8	29.8	40.6	40.6	30.4	29.8
Grain size d_s [mm]	[5, 5.5]	[2.5, 4]	[4, 5]	[2, 2.5]	[4, 4.5]	[3, 4]	[2, 2.5]	[2, 2.5]
Tilt range ϕ [deg]	[−1.6, 1.6]	[−0.9, 1.3]	[−1.5, 1.7]	[−1.0, 1.1]	[−2.1, 1.2]	[−1.5, 1.8]	[−1.0, 1.2]	[−0.9, 1.2]
Number of movies	60	30	60	30	20	30	30	30
Diffusivity								
D_{hard} [cm^2 s^{-1}]	2.3 ±0.7	2.9 ±0.5	1.8 ±0.8	1.8 ±0.6	0.9 ±0.4	1.4 ±0.3	2.3 ±0.3	2.8 ±0.7
D_{soft} [cm^2 s^{-1}]	4.4 ±3.2	3.9 ±3.1	5.4 ±3.7	3.5 ±2.2	3.3 ±1.7	3.8 ±2.1	3.0 ±2.0	4.6 ±2.9
Horizontal velocity (RMS)								
$v_{\mathrm{rms,\,hard}}$ [cm s^{-1}]	10.5 ±3.1	10.7 ±2.0	9.0 ±4.6	9.2 ±3.3	6.8 ±2.4	8.4 ±3.6	9.9 ±1.6	11.3 ±3.5
$v_{\mathrm{rms,\,soft}}$ [cm s^{-1}]	14.6 ±3.2	12.8 ±3.0	14.5 ±4.0	12.2 ±1.9	11.7 ±3.4	11.9 ±3.4	11.4 ±2.6	13.9 ±2.6

variability of their size is reported in Tables I and II as the mesh size of the two sieves in between which the grains of a given class are collected (except for runs I, L, M, and N, for which the grains were hand-picked, and their size estimated from pictures). The grains' roughness causes them to bounce in random directions—by contrast, smooth beads tend to maintain their direction over a few jumps. As they bounce over the vibrating plate, the grains typically jump up to a few millimeters above the plate's surface, but we did not measure this height directly.

We used a top-view camera (Canon EOS 600D) to record the horizontal trajectories of the grains with a series of one-minute-long movies at a frame rate of 50 Hz, which is just fast enough to keep a clear view of individual grains [Fig. 1(b)]. The camera is controlled with the Linux library `gPhoto2` [15]. It records images of size 1280 × 720 px, which corresponds to a spatial resolution of 0.14 mm px^{-1} on the vibrating surface. The grains appear as whitish over a green or pink background, and we can thus use the saturation of the image as an indicator of the grain's presence. After smoothing numerically the saturation frame over a distance of one grain size (Gaussian filter), the grains' centers appear as clear maxima. To track individual grains, we need to keep their number low enough that their identity from one image to the next remains unambiguous (about 5 grains for each experiment in practice). Then, we finally use the Munkres algorithm of the `scikit-image` Python library to reconstruct the trajectories of every grain for the duration of a movie [dashed lines in Fig. 1(b)] [16–18]. Trajectories are broken when two grains come close to each other, but these events are rare enough to leave us with many long trajectories. These data are freely available online [19].

Finally, the loudspeaker, vibrating plate and camera are all fixed on a vertical rectangular frame held by two hinges which can rotate about the x axis of Fig. 1(a). A stepper motor (Zaber NM23A200), controlled by an Arduino Motor Shield, turns a micrometric screw which pushes the frame away from the vertical, and thus tilts the vibrating disk with respect to the horizontal. We digitally record this tilt with a capacitive inclinometer (Meiri ME 26410), the output of which is converted numerically at a resolution of 0.01° (Microchip MCP3424). This inclination adds a tunable potential force to the grains' dynamics, which makes this setup suitable to run a BL motor [12]. Here, we will use this feature only to measure the mobility of the bouncing grains.

During a typical experiment, we start the function generator, and observe the motion of four or five grains over the vibrating disk. We increase the vibration amplitude until the grains start to move randomly (when the amplitude is too low, the grains appear to hover smoothly over the disk's surface [3]). We then check with the naked eye that the grains' density is symmetric about the rotation axis of the frame (x axis), which allows us to finely tune the tilt of the disk and find its horizontal position. This manual procedure gave us better results than trying to find the zero of the inclinometer. We then record the number of movies we wish to use for these experimental conditions (typically a series of five movies, with a

TABLE II. Experimental parameters for the second series of experiments. The substrate is either soft or hard, but always uniform [Figs. 2(a) and 2(b)]. The disk was kept horizontal for these runs, and vibrated at a frequency of 30 Hz. The vibration amplitude was varied, diffusivity and root-mean-square velocity changed accordingly. Brackets indicate sieve sizes for d_s, whereas gray numbers indicate size variability for hand-picked grains.

Run	I	J	K	L	M	N
Substrate	hard	soft	hard	soft	hard	soft
Grain size d_s [mm]	1.5 ±0.2	[2.5, 4]	[2.5, 4]	6 ±0.6	6 ±0.6	1.5 ±0.2
Number of movies	41	24	55	42	41	50
Acceleration range $A\omega^2/g$	[1.6, 2.7]	[1.4, 2.1]	[0.8, 2.7]	[1.3, 2.5]	[1.7, 2.9]	[1.5, 1.8]

30 s pause between them). Finally, we change the vibration amplitude or tilt, and repeat.

In the present paper, we use two distinct series of experiments. During the first series (runs A to H, Table I, also used in the companion paper [12]), we did not measure the vibration amplitude A, but it remained visibly less than 1 mm. These runs featured a heterogeneous substrate, as shown in Fig. 2(c), over which the statistical equilibrium we investigate in the present paper can establish itself. The setup was tilted to different angles, and the combination of a heterogeneous substrate and an external force formed a BL motor—the subject of the companion paper [12]. Here, we use this external force only in Sec. II D, to measure the mobility of the bouncing grains.

Runs I to N (Table II), by contrast, were specifically devised for the investigation of the grains' microscopic dynamics. They were made on a homogeneous substrate [hard or soft, Figs. 2(a) and 2(b)], which allowed better diffusivity measurements, especially over the soft polymer which, in runs A to H, extended only over a small area. The vibrating disk remained horizontal in runs I to N, and we also affixed a digital accelerometer on the vibrating disk (Joy-It MMA8452Q), and measured the vibration amplitude to be typically about $A \sim 0.5$ mm (Table II). The dimensionless acceleration of the plate, $A\omega^2/g$ where $\omega = 2\pi\nu$ is the angular frequency and g is the acceleration of gravity, was thus of order one in all our experiments. This combination of amplitude and frequency was set by trial and error but, in retrospect, it can be justified as follows. If the dimensionless acceleration is less than one, the grains do not leave the plate, and the diffusivity vanishes. Conversely, far above this threshold, the diffusivity depends only weakly on the type of substrate [5], thus impairing the heterogeneity we are after.

In the next section, we introduce a simple model to represent the motion of the bouncing grains, and test it against these two data sets.

B. Ballistic trajectory and random walk

When the vertical acceleration of the vibrating plate exceeds that of gravity ($A\omega^2 \gtrsim g$), the grains start bouncing over its surface, in a fashion that is similar to what happens in a regular Chladni experiment [5,6]. To the naked eye, the frequency of their bouncing is lower than that of the vibrating disk, and their horizontal motion seems erratic. The latter is confirmed by particle tracking [Fig. 3(a)]: The horizontal trajectory of a grain is irregular and, over time, seems to explore the entire disk over which it is confined.

To ground this observation in measurements, we compute the mean-square displacement of a collection of trajectories, namely

$$\sigma^2 = \langle \|\mathbf{x} - \mathbf{x_0}\|^2 \rangle, \tag{4}$$

where $\mathbf{x}$ is the position of a grain at a given time, $\mathbf{x}_0$ its position at the onset of its trajectory, and $\langle\cdot\rangle$ is the ensemble average, which we approximate with the average over our data set. To mitigate the influence of the walls, we cut each trajectory wherever it comes too close to a wall, and treat the resulting pieces as independent trajectories. The square displacement σ^2 is averaged over many trajectories, and we can plot it as a function of its duration t [Fig. 3(b)]. As expected, the square displacement grows with time, and this growth becomes linear after about 0.05 s. Beyond about 0.2 s, however, the displacement becomes comparable to the box size [dotted line in Fig. 3(b)], and our measurements become meaningless beyond this point.

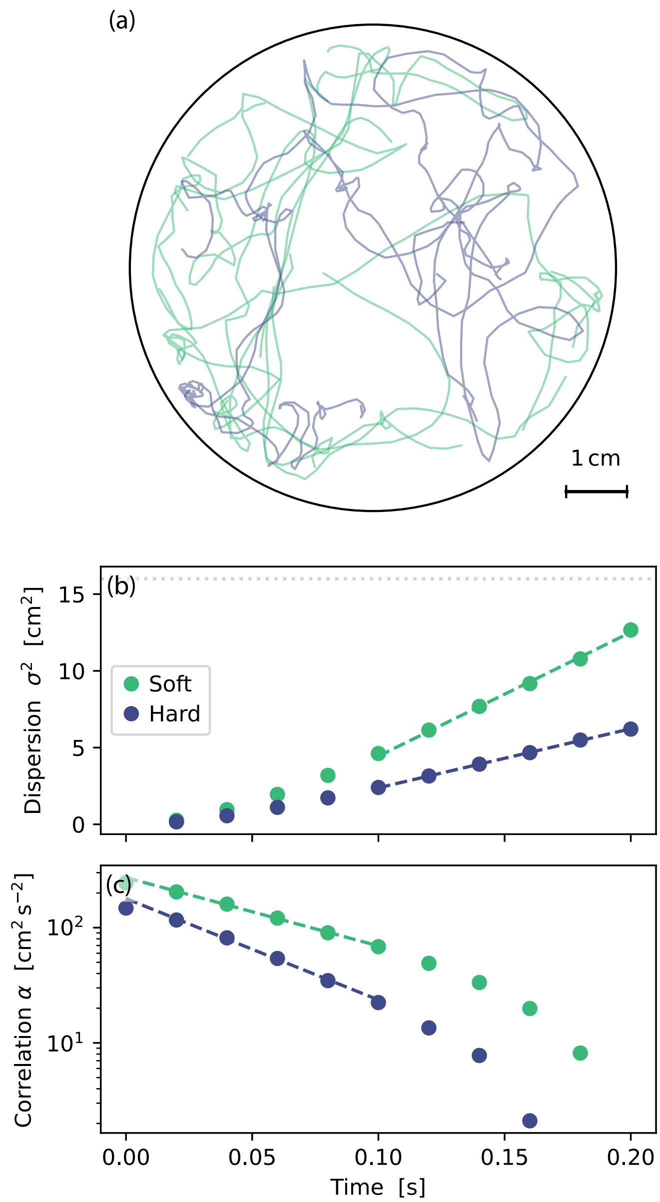

FIG. 3. (a) Examples of trajectories over hard and soft disk (runs L and M, $f = 30$ Hz, $d_s = 6$ mm, dimensionless acceleration $A\omega^2/g = 1.6$ and 1.9, respectively). (b) Average dispersion σ^2 of trajectories with time (dots). Dashed lines show linear fits with slope $4D$. Hard: $D = 9.6\,\mathrm{cm^2\,s^{-1}}$; soft: $D = 20.2\,\mathrm{cm^2\,s^{-1}}$. Dotted gray line indicates box size R^2. (c) Autocorrelation function of the grains' velocity (dots). Dashed line shows exponential fit, with amplitude from Eq. (5). Hard: $D = 8.8\,\mathrm{cm^2\,s^{-1}}$, $\tau_c = 0.049$ s; soft: $D = 19.9\,\mathrm{cm^2\,s^{-1}}$, $\tau_c = 0.073$ s.

We interpret the linear regime as the signature of a random walk, and therefore the slope of this relation as a measurement of the corresponding diffusivity. For run M, for instance, we find $D = 9.6\,\mathrm{cm^2\,s^{-1}}$ over a hard substrate. For comparison, run L is made under similar circumstances, but over a soft elastomer disk; we then find $D = 20.2\,\mathrm{cm^2\,s^{-1}}$—about twice the diffusivity over the hard substrate. Diffusivity also depends on grain size and plate acceleration, but we will not investigate these dependencies here (Appendix A).

If the random-walk interpretation is correct, then the faster-than-linear growth of the square displacement that occurs before the linear regime corresponds to the ballistic regime, that is, to the free trajectory of a grain before it hits the substrate. Accordingly, we expect that the correlation time τ_c of a trajectory be comparable to the crossover time between these two regimes.

To check this, we now compute the autocorrelation function of the horizontal velocity, $\alpha(t) = \langle v(t)\, v(0)\rangle$, and plot it as a function of time [Fig. 3(c)]. We find that it can be represented by an exponential decay, at least for a correlation time of less than about 0.1 s. The characteristic time of this decay is $\tau_c = 0.049$ s for run M (0.073 s for run L), which is comparable to the cross-over time visible in Fig. 3(b). For completeness, we now use the autocorrelation function to estimate again the diffusivity, by invoking the Green-Kubo relation:

$$D = \int_0^\infty \alpha(t)\, \mathrm{d}t. \tag{5}$$

For run M, for instance, we find $D = 8.8\,\mathrm{cm^2\,s^{-1}}$ with this method, to be compared with $D = 9.6\,\mathrm{cm^2\,s^{-1}}$ from the linear fit of the dispersion as a function of time [Figs. 3(b) and 3(c)]. We generally obtain values differing by less than 10 % from the dispersion measurements, which indicates that, over a flat uniform surface, bouncing grains diffuse randomly. Based on the decorrelation time of their random walk, we expect that their jumps typically last a few hundredths of a second.

We now wish to interpret these observations within a simple theoretical framework, in which we will favor clarity over exactness. In particular, we assume that the randomness of the grain's motion is limited to its rebounds, during which the roughness of its surface diverts it from their initial horizontal course. In between jumps, accordingly, we expect its trajectory to follow a ballistic parabola. The duration τ of a jump of height h then reads

$$\tau = 2\sqrt{\frac{2h}{g}}. \tag{6}$$

Interpreting the autocorrelation decay time τ_c as the typical jump duration τ, this expression yields a bouncing height of $h \sim 3$ mm. This order of magnitude matches the estimate that one can make with the naked eye.

Based on the same assumptions, the horizontal extension ℓ of a step is

$$\ell = v\,\tau, \tag{7}$$

where v is the norm of the grain's horizontal velocity. In our simplistic model, this velocity is a constant, but of course in practice it varies from one bounce to the next. To get a sense of scales, we will later identify it with the root-mean-square velocity we measure in experiments, but this will only be a rough approximation. Returning to the model, we neglect the friction of air, and accordingly assume that energy is conserved as long as the grain is detached from the plate. We can thus relate the vertical velocity of the grain at the onset of a jump to the height h of that jump:

$$v = \frac{\sqrt{2gh}}{\tan\theta}, \tag{8}$$

where θ is the initial angle of the trajectory with respect to the horizontal [Fig. 1(c)]. We do not expect any specific value for the angle θ based on general principles; we rather expect it to depend on microscopic details such as the shape of the grains. Despite its mundane origin, this angle determines the partition of energy between vertical and horizontal directions—equipartition requires $\theta = 45°$.

Overall, Eqs. (6) to (8) leave us with two free parameters: The bouncing angle θ, which we cannot measure directly, and the horizontal velocity of a grain v, which we can measure with particle tracking. We do so in the next section.

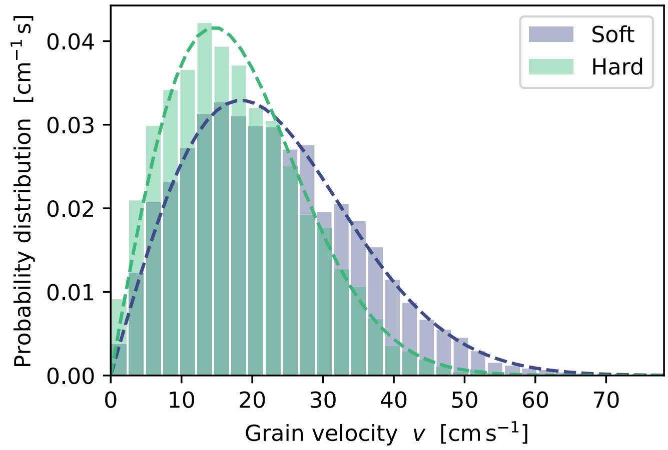

FIG. 4. Velocity distribution over a uniform substrate (runs L and M, $f = 30$ Hz, $d_s = 6$ mm, dimensionless acceleration $A\omega^2/g = 1.6$ and 1.9, respectively). Colors correspond to type of substrate. Bars: experimental probability distribution. Dashed lines: Maxwell-Boltzmann distribution with the same root-mean-square value ($v_{\mathrm{rms}} = 26.1\,\mathrm{cm\,s^{-1}}$ over the soft substrate, and $20.6\,\mathrm{cm\,s^{-1}}$ over the hard substrate).

C. Maxwell-Boltzmann distribution

Using the trajectories resulting from the grain tracking procedure, we can compute the horizontal velocity v of a grain between two camera frames. The frame rate of the camera is accurate, so the uncertainty of this measurement stems from the grains' position only. The latter is of the order of a pixel, which yields an uncertainty of about $1\,\mathrm{cm\,s^{-1}}$. Figure 4 shows the distribution of the grains' velocity for experimental runs L and M. We find that these distributions are broad and, within the uncertainty of our measurements, they are well represented by a two-dimensional Maxwell-Boltzmann distribution, that is

$$\rho_v = \frac{2v}{v_{\mathrm{rms}}^2} e^{-(v/v_{\mathrm{rms}})^2}, \tag{9}$$

where $v_{\rm rms} = \sqrt{\langle v^2 \rangle}$ is the root-mean-square of the horizontal velocity, measured for all the movies in an experimental run that were shot with the same vibrational acceleration. In other words, like in an ideal gas, the probability density of a grain in the two-dimensional velocity space decreases exponentially with its kinetic energy. Under otherwise similar conditions, the grains are faster over the soft substrate ($v_{\rm rms} \approx 26.1\,{\rm cm\,s^{-1}}$) than over the hard disk ($20.6\,{\rm cm\,s^{-1}}$). In that sense, they are more energetic over the elastomer, as one would intuitively infer from their higher diffusivity (Sec. II B).

Invoking the energy balance during a jump, in the form of Eq. (8), and identifying the horizontal velocity of our simple model with the root-mean-square velocity, we find that the bouncing angle is about $\theta \sim 50^\circ$ on the hard substrate (Abramian *et al.* [5] measured 53° in their Chladni experiment). We will get another estimate of this angle in Sec. II D, but this value is certainly compatible with direct observation of our bouncing grains.

D. Temperature

We now turn to the randomness associated with a grain's bouncing. We hypothesize that a grain loses memory at each bounce, and that it takes off from the vibrating plate in any direction with equal probability. Projected on the vibrating plate, that is, on the (x, y) plane, the trajectory of a grain is thus a two-dimensional random walk with a correlation time τ, and a characteristic step size $\ell = v\tau$. On average, this random walker diffuses over the plate with diffusivity

$$D = \frac{\ell^2}{4\tau} = \frac{v^3 \tan\theta}{2g}. \tag{10}$$

We can test this expression with experimental grain trajectories, assuming that all its parameters are constant, including the bouncing angle θ.

To do so, we use experimental runs A to H, wherein the grains bounce over a heterogeneous substrate. This allows us to measure the diffusivity D and the root-mean-square velocity $v_{\rm rms}$ over the two substrates at exactly the same vibrational acceleration, provided we distribute the data into two bins corresponding to the hard and soft substrates. In addition, we changed the tilt angle of the substrate for these runs, and this will allow us to measure the mobility in the same runs.

Identifying the constant velocity of the model, v, with the root-mean-square velocity that we measure in experiments, $v_{\rm rms}$, we find that diffusivity consistently increases with velocity in runs A to H [Fig. 5(a)]. The associated relation is compatible with an exponent of 3 (a least-squares fit in log-log space yields an exponent of 3.3 ± 0.5). Assuming the exponent is indeed 3, we can fit Eq. (10) to the data, and we thus find a bouncing angle of $\theta \approx 75^\circ \pm 6^\circ$. This value is significantly different from the estimate of Sec. II C.

Here we face the limitations of our order-of-magnitude model. The bouncing angle θ and the velocity v vary from one bounce to the next, and should be thought of as random variables. Their mean or root-mean-square values, therefore, cannot be directly injected into Eqs. (8) and (10)—hence the discrepancy between the two estimates. A better model wherein each parameter has its own distribution can be envisioned, but our experimental setup gives us no access to the

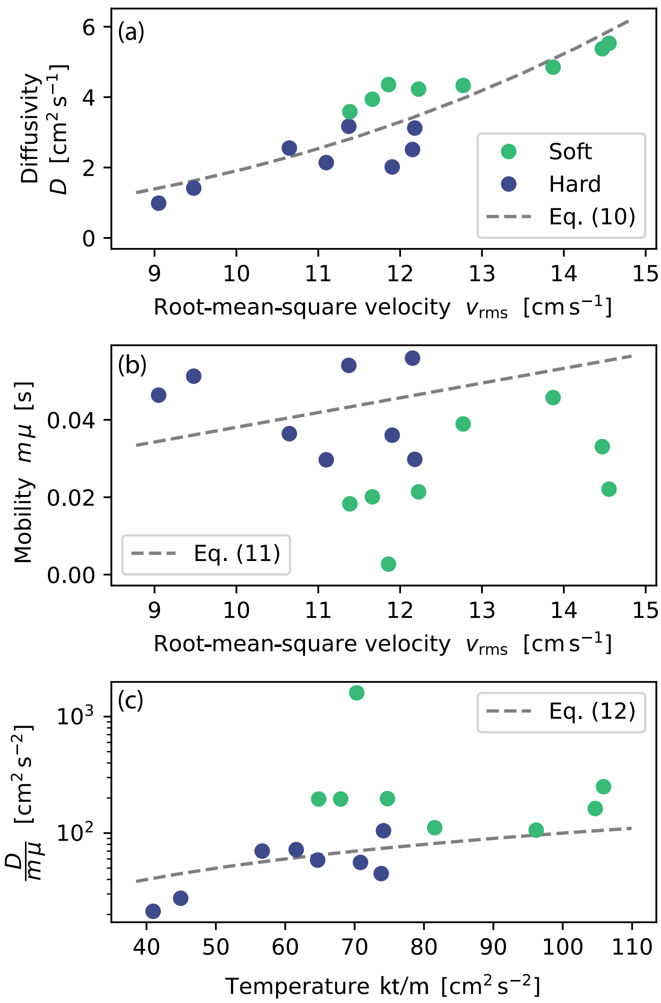

FIG. 5. Empirical evaluation of the bouncing-grain model (Sec. II, runs A to H only). (a) Diffusivity as a function of root-mean-square velocity. Dashed line: Eq. (10) with a bouncing angle of $\theta = 75^\circ$ (fitted to data). (b) Mobility as a function of root-mean-square velocity. The product $m\mu$ is independent of the mass m of a grain. Dashed line: Eq. (11) with $\theta = 75^\circ$. (c) Fluctuation-dissipation relation. Dashed line: one-to-one relation, Eq. (12).

angle θ, and such a model would therefore be overkill. About the bouncing angle, we can only say with some confidence that its tangent is of order one. Unfortunately, this leaves us without any definitive answer about the equipartition of energy between the horizontal and vertical directions, which we cannot rule out. We would find it surprising, however, that equipartition be always satisfied, thus fixing the bouncing angle to 45° regardless of the grains' shape and the type of substrate.

To further the comparison with microscopic thermodynamics, we now investigate the inseparable companion of diffusivity—mobility. If a horizontal force f acts upon a grain of mass m, then the latter will accelerate in response to the force as long as it is detached from the plate. Over the duration τ of its flight, it acquires an additional velocity equal to $f\tau/m$. Since we assume that, at each bounce, the grain's velocity is reset to zero, the acquired velocity averages over the duration

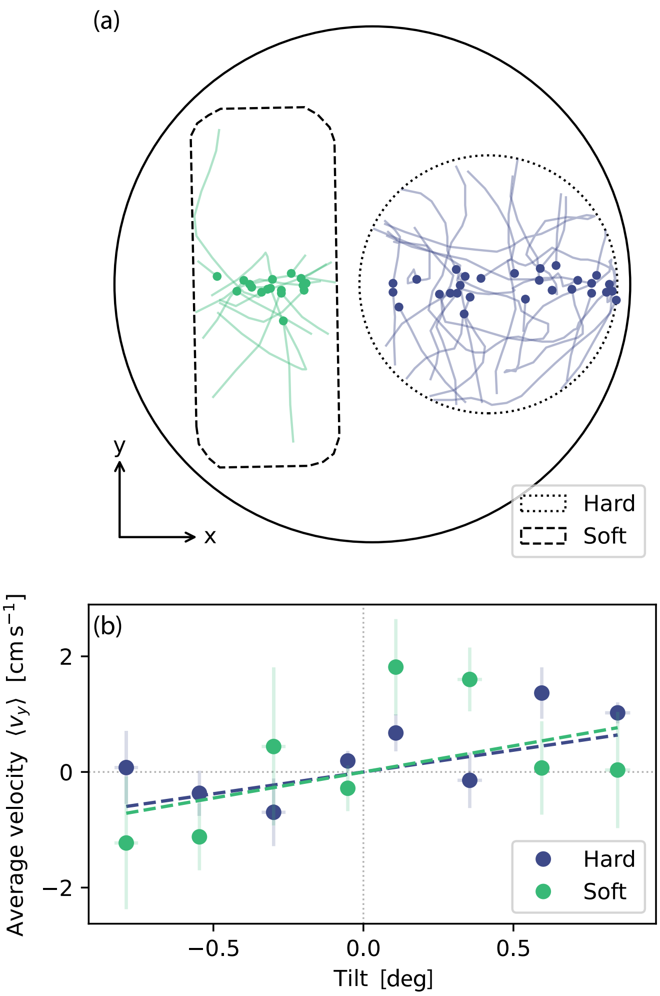

FIG. 6. Measurement of mobility in the experiment. (a) Examples of truncated trajectories, all starting near the $y = 0$ line, and split into two subdomains corresponding to hard and soft substrates (run C). Each trajectory starts from the dot. (b) Average velocity of the truncated trajectories as a function of the tilt angle for run C. For each domain (soft and hard) the data are distributed into nine bins and averaged therein. Error bars show standard deviation. The slope of the linear fit to the data is an estimate of the mobility μ (dashed lines). We find $mg\mu = 52\,\mathrm{cm\,s^{-1}}$ over the soft pad, and $mg\mu = 43\,\mathrm{cm\,s^{-1}}$ over the hard disk.

τ of a flight to $f\tau/(2m)$. Defining the mobility μ of the grain as the ratio of this velocity to the force that induces it, we find

$$m\mu = \frac{\tau}{2} = \frac{v}{g}\tan\theta. \tag{11}$$

We can measure the mobility by applying a force on bouncing grains, and then track their trajectories. The ratio of the average velocity of a grain to the intensity of the force that drives it is the mobility.

To generate a horizontal force, we tilt the vibrating substrate with respect to a horizontal, and measure its angle (runs A to H). As a rough estimate of the average velocity $\langle v_y \rangle$ along the y axis (the direction of the force), we first distribute the trajectories into two subdomains, namely the soft pad, and a circular domain of similar area over the hard disk [Fig. 6(a)]. We now need to perform a Lagrangian measurement of the velocity (as opposed to the average velocity of a population of grains considered in a fixed domain). This measurement is valid only away from any boundary.

To get a Lagrangian average, we truncate the trajectories where they cross the x axis, and then where they leave the domain of interest. Finally, we average the velocity over those truncated trajectories, and plot the resulting value as a function of the tilt of the plate [Fig. 6(b)]. The data appear scattered around a linear trend, the slope of which is an estimate of mobility (actually, an estimate of $mg\mu$).

We are now ready to test Eq. (11) against experiments provided, again, that we identify the typical velocity of a grain v with the root-mean-square velocity v_{rms}. We then plot the product $m\mu$ as a function of the root-mean-square velocity [Fig. 5(b)]. No free parameter remains at this stage, and we can directly plot the linear relation of Eq. (11) on the same plot. For a bouncing angle $\theta = 75^\circ$, this expression appears compatible with the data, despite a large scatter. For unknown reasons, run F (soft substrate) appears as an outlier.

Finally, following classical convention, we define the macroscopic temperature kT as the ratio of diffusivity to mobility:

$$kT = \frac{D}{\mu} = \frac{mv^2}{2}. \tag{12}$$

Unsurprisingly, in the present theory, the macroscopic temperature of our bouncing grains is just their kinetic energy in the horizontal plane. This was to be expected for such a simple model; we now test this relation against observations.

Using the grains' trajectories, we estimate independently their diffusivity D, their mobility μ and their mean-square velocity v_{rms}^2. Identifying the latter as the temperature (up to an $m/2$ coefficient), we can test the fluctuation-dissipation relation, in the form of Eq. (12), without any reference to the bouncing angle [Fig. 5(c)], nor to any other fitting parameter. Again, we find a large scatter around the line corresponding to the exact relation, with run F still an outlier—the result, perhaps, of our fragile measurement of the mobility.

Overall, however, the data appear to accord with the fluctuation-dissipation relation. This allows us to consistently define a macroscopic temperature, either as the ratio of diffusivity to mobility, or as the average kinetic energy of the grains (in the plane of the vibrating substrate). In that sense, the bouncing grains are a sound analog of molecular thermodynamics; they might prove useful, for instance, for the teaching of elementary statistical physics. Their macroscopic size, and the simplicity of the setup, might foster a developing intuition for thermodynamics.

The analogy with molecular thermodynamics, however, cannot be pushed too far. As we will see in Sec. III, indeed, it breaks down when the temperature is not uniform—and the diffusion law is at the core of this breakdown.

III. ITÔ DIFFUSION

A. Non-Fickian diffusion

So far, we only considered a random walk over a uniform substrate. Although we did use data from heterogeneous experiments, we split it into two substrate classes and treated

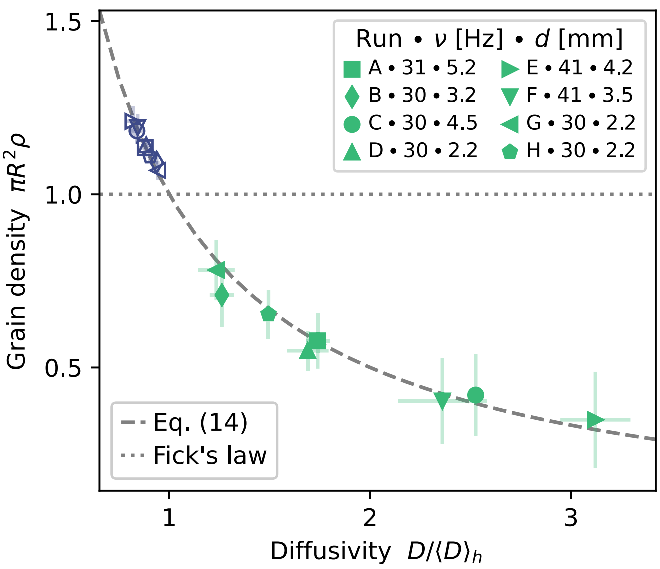

FIG. 7. Grain density over a horizontal, heterogeneous substrate, as a function of dimensionless diffusivity. Each experimental run is represented by two data points (Green filled markers: soft pad; Empty blue markers: hard disk). Vertical error bars indicate standard deviation over successive movies. Horizontal error bars correspond to different estimates of the diffusivity ($2D = \langle y^2/t\rangle$ or $\langle y^2\rangle/\langle t\rangle$).

these classes independently. We now investigate in detail the behavior of bouncing grains over a heterogeneous substrate [Fig. 2(c)]. Their diffusivity is now a function of space, and so is the temperature, since the two quantities are related by Eqs. (10) and (12), which we can recombine into

$$kT = \frac{m}{2^{1/3}}\left(\frac{gD}{\tan\theta}\right)^{2/3}. \tag{13}$$

We thus exit the realm of thermodynamic equilibrium.

In the present paper (and its companion [12]), we follow Abramian *et al.* [5] and claim that Eq. (2) is a better representation of the diffusion of bouncing grains than Fick's law (1). Although a formal derivation of this expression from first principles (i.e., from Newton's laws) is outside the scope of the present paper, we support this claim with three arguments. Namely, (i) the inevitability of Eq. (2) for an explicit, unbiased random walk [10,20,21]; (ii) the notion of bouncing, which implies that the external noise acts intermittently, at the onset of each jump (Sec. II); (iii) the heterogeneity of the statistical equilibrium reached in experiments, to which we now turn.

If Fick's law (1) were to hold on a heterogeneous substrate, then the grains would distribute themselves uniformly in statistical equilibrium ($\mathbf{j} = 0$). Instead, Eq. (2) yields

$$\rho = \frac{\langle\rho\rangle_a\langle D\rangle_h}{D} = \frac{\langle D\rangle_h}{\pi R^2 D} \tag{14}$$

at statistical equilibrium, where $\langle\cdot\rangle_h$ is the harmonic average over the vibrating disk, whereas $\langle\cdot\rangle_a$ is the arithmetic average. Both are space averages, and $\langle\rho\rangle_a = 1/A$, where A is the area of the domain. Telling the two theories apart is now straightforward—one simply needs to measure the density of the bouncing grains in an experiment at statistical equilibrium, and plot it as a function of diffusivity. Figure 7 leaves no ambiguity as to which theory better accounts for observations [Eq. (14) requires no fitting parameter, and Fick's law predicts $\rho\pi R^2 = 1$].

In the next section, we investigate the difference between Eq. (2) and Fick's law, and the microscopic origin of these relationships.

B. Drift

To underline the peculiarity of Eq. (2), we momentarily turn to numerical simulations. As it turns out, the simulation of a random walk that obeys Eq. (2) is simpler than one that yields Fick's law. One simply needs to use a random generator whose standard deviation depends on the current position of the walker, add its output to the walker's position, and repeat. Mathematically, one then simulates an explicit, unbiased random walk [10]—in mathematical terms, a martingale.

Figure 8 shows the results of such a simulation in one dimension. For illustration, we choose a step length that varies with the position x of the particle according to

$$\ell = \sqrt{1 - 0.9\sin(2\pi x)}\,; \tag{15}$$

so that diffusivity, $D = \ell^2/(2\tau)$, depends sinusoidally on space [we assume that the time step is constant, Fig. 8(a)]. The simulation is made periodic, and thus x is confined to the interval [0,1]. Starting with a uniform distribution of walkers, we find that they quickly gather around the diffusivity minimum, and their distribution then reaches a heterogeneous steady state [Fig. 8(b)].

To put Eq. (14) to the test, we simply compare the (normalized) equilibrium distribution of the walkers with $\langle D\rangle_h/D$, which is a function of x [dashed line in Fig. 8(b)]. This expression matches the numerical distribution, thus showing that this simple simulation behaves like bouncing grains.

As the grains gather around the diffusivity minimum, their center of mass shifts. By definition, its position is $\langle x\rangle$, where $\langle\cdot\rangle$ is the ensemble average (formally, $\langle\cdot\rangle = \langle\rho\,\cdot\rangle_a$ when the system is ergodic). Initially, the grains are uniformly distributed over the domain, that is, $\langle x\rangle = 0.5$. As steady state is reached, this position shifts to

$$\langle x\rangle = \frac{\int x/D\,\mathrm{d}x}{\int 1/D\,\mathrm{d}x} \approx 0.322, \tag{16}$$

when steady state is reached, as visible in Fig. 8(c). This observation is just a direct consequence of Eq. (14) but, when looked upon from a slightly different perspective, it can prove illuminating.

To see this, let us now release the walker from the domain [0,1] and assume, instead, that it roams through an infinite, periodic diffusivity field, still defined by Eq. (15). One can think of a grain bouncing on an infinitely long, one-dimensional Chladni plate. As it turns out, the numerical simulation of this problem is exactly the same as before, only without folding the particle's position over a single period when we calculate its average position. We then find that the mean position $\langle x\rangle$ of the particle does not change [Fig. 8(c)].

This apparent paradox is yet another way to distinguish Eq. (2) from Fick's law. Based on the former, indeed, the

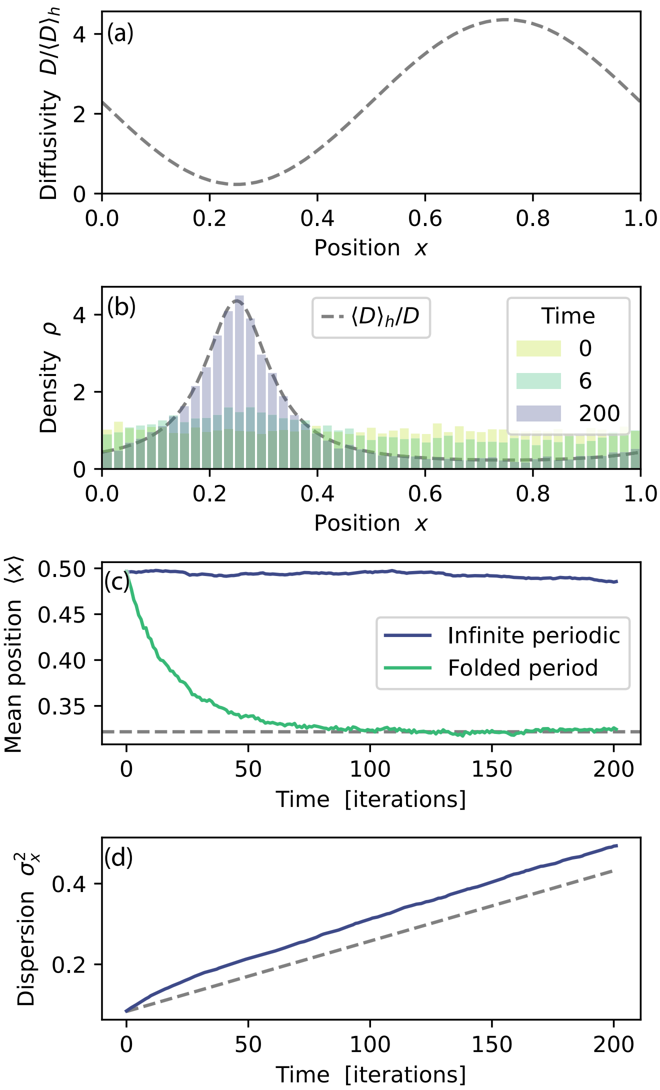

FIG. 8. One-dimensional random walk simulation with heterogeneous diffusivity ($D \propto \ell^2$, Eq. (15), with 10^4 walkers). (a) Diffusivity profile. (b) Position histogram at three different times, with folded periods (the walker's position is $x \mod 1$). Dashed line shows theory, Eq. (14). (c) Evolution of the average position of the walkers. Dark blue line: Infinite periodic system. Light green line: periods are folded over the interval [0,1]. Dashed line shows the theoretical value, Eq. (16). (d) Dispersion of the walkers. Dashed line shows effective diffusion, Eq. (20).

Smoluchowski equation reads

$$\frac{\partial \rho}{\partial t} = \frac{\partial^2}{\partial x^2}(D\rho), \tag{17}$$

to which we need to adjoin boundary conditions. In the case of a walker in an infinite domain, the probability density and current vanish at infinity—provided the initial distribution is compact. Therefore, the average position of the particle reads

$$\frac{\partial \langle x\rangle}{\partial t} = \int_{-\infty}^{\infty} x \frac{\partial^2}{\partial x^2}(D\rho)\mathrm{d}x = -[D\rho]_{-\infty}^{\infty} = 0, \tag{18}$$

where we have integrated by parts the first integral. This result accords with our simulation, but it contrasts with Fick's law, which induces a finite drift in a heterogeneous diffusivity field (Appendix B).

In the simulation presented here, the length of a step depends only on the walker's position at the onset of the jump. A direct consequence of this fact is that, at the onset of each step, the walker can go either left or right with the same probability, and with the same step length and velocity. Therefore, in the absence of any external force, its average position at step $i+1$ is the same as at step i—the definition of a martingale. Unless some boundary is reached, therefore, the average position of a grain cannot change [Fig. 8(c), dark blue line]. In that sense, this process appears as the natural generalization of a random walk for heterogeneous diffusivity (we will mitigate this statement in Sec. III C).

By contrast, when we introduce periodic boundaries in Eq. (18), the integration by parts yields finite constants which allow the average position of the particle to drift [Fig. 8(c), light green line]. This is because the initial distribution, mapped on an infinite periodic domain, now extends to infinity—it is not compact any more.

Returning to the infinite domain, we note that, although the average position of the walker does not change, it still disperses as diffusion goes on. Using again the Smoluchowski equation (17) to get the variance of the particle's position, we find

$$\begin{aligned}\frac{\partial \sigma_x^2}{\partial t} &= \int_{-\infty}^{\infty} x^2 \frac{\partial^2}{\partial x^2}(D\rho)\mathrm{d}x \\ &= 2\int_{-\infty}^{\infty} D\rho\,\mathrm{d}x = 2\langle D\rangle.\end{aligned} \tag{19}$$

Once the walkers have diffused over many periods of the diffusivity field, we may assume that their distribution is locally close to the equilibrium distribution (3). Accordingly,

$$\sigma_x^2 \sim 2\langle D\rangle_h t \tag{20}$$

and the effective diffusion coefficient is $\langle D\rangle_h$. This expression accords with numerical simulations [Fig. 8(d)], and with the general treatment of this problem recently proposed by Giordano and Blossey [22]. The fact that the effective diffusivity is the harmonic mean of diffusivity is yet another signature of the special kind of diffusion that Eq. (2) stands for.

This problem is reminiscent of a travel at varying velocity, the duration of which involves the harmonic mean of the velocity. Because the harmonic mean is always less than the arithmetic mean, the fastest diffusion of bouncing grains happens for uniform diffusivity, just like constant speed makes for the fastest travel. Conversely, introducing heterogeneity in the diffusivity creates traps which slow down the diffusion of the walker.

C. Markov chain

We now treat the bouncing of a grain explicitly as a discrete Markov process, wherein the length and duration of a jump depend only on the grain's starting position; in that sense, it is explicit. In one dimension and setting the initial position to

$x = 0$, we may thus write, for N steps,

$$x_N = \sum_{i=1}^{N} \ell(x_i)\, w_i, \tag{21}$$

where w_i is a random variable of vanishing mean and variance unity, which is independent of the grain's position. For illustration, we choose here $w_i = \pm 1$. Because the length of a jump depends only on the position x_i, and not on its next position x_{i+1}, this sum converges to an Itô integral in the limit of infinitesimal jumps. For this reason we hereafter refer to this process as "Itô diffusion."

By referring to an Itô process, we implicitly contrast it with the Stratonovich integral, a discrete version of which would read

$$x_N = \sum_{i=1}^{N} \frac{\ell(x_i) + \ell(x_{i+1})}{2}\, w_i, \tag{22}$$

and with the anti-Itô integral—sometimes called "isothermal" or named after Hänggi [23]—which reads

$$x_N = \sum_{i=1}^{N} \ell(x_{i+1})\, w_i. \tag{23}$$

Both the drift-free Stratonovich and anti-Itô sums immediately appear unsuited to the random bouncing of a grain: How would the grain know on which substrate it will land at x_{i+1} before hitting it [24]? (In the continuous limit, however, both yield legitimate descriptions of different microscopic dynamics.) This question is of little relevance when the diffusivity is uniform, as the three sums—Itô, Stratonovich, and anti-Itô—converge to the same integral when the characteristics of the steps are uniform. However, when these characteristics depend on space, choosing Eq. (21), Eq. (22), or Eq. (23) changes the macroscopic diffusion process, even in the limit of a vanishing step length [10]. The Itô integral yields Eq. (2), whereas the anti-Itô one corresponds to Fick's law. As for the Stratonovich integral, it lies in between the two, and yields $\mathbf{j} = -\sqrt{D}\,\nabla(\sqrt{D}\rho)$. Van Kampen [[25], p. 231] noted that this point, although well established mathematically, often remains a source of confusion.

We now return to Eq. (21), which defines the displacement of the grain, and complement it with its counterpart in time, namely,

$$t_N = \sum_{i=1}^{N} \tau(x_i), \tag{24}$$

where t_N is the duration of the trajectory. This expression, again, corresponds to an Itô process. An unusual fact about it is that, if the step duration τ is not constant, then the number of steps N at a given time depends on the grain's trajectory—a consequence of Eqs. (21) and (24) being discretized in terms of individual bounces.

Let us first check that, on average, the grain does not move. By definition,

$$\langle x_N \rangle = \sum_{i=1}^{N} \langle \ell(x_i)\, w_i \rangle, \tag{25}$$

and, since w_i is uncorrelated with the grain's position,

$$\langle \ell(x_i)\, w_i \rangle = \langle \ell(x_i) \rangle \, \langle w_i \rangle = 0. \tag{26}$$

Thus, for a fixed number of jumps N, the mean displacement $\langle x_N \rangle$ vanishes. It is not obvious, however, that this result holds for a fixed physical time t. Because τ varies from one jump to the next, indeed, the total number of jumps N depends on the trajectory, according to Eq. (24). The above derivation, however, can still serve as a heuristic explanation of why the mean position of an isolated Itô random walker does not change, as per Eq. (18).

As is customary for a random walk, we can also compute the variance of the grain's position:

$$\langle x_N^2 \rangle = \left\langle \left(\sum_{i=1}^{N} \ell(x_i)\, w_i \right)^2 \right\rangle = \left\langle \sum_{i=1}^{N} \ell(x_i)^2 \right\rangle, \tag{27}$$

where the cross terms vanish because the conditional mean of the increments vanish (they are orthogonal in expectation). We now introduce the time step in the above sum:

$$\langle x_N^2 \rangle = 2 \left\langle \sum_{i=1}^{N} D(x_i)\tau(x_i) \right\rangle = 2 \langle \bar{D}\, t_N \rangle, \tag{28}$$

where an overlined quantity is time-averaged over a trajectory. Again, this equation is exact for a fixed number of steps, but its validity when the physical time is fixed is unclear. In the continuous limit, however, In the continuum limit, however, one expects Eq. (28) to become $\langle x^2(t) \rangle = 2t \langle \bar{D} \rangle$, which is the time-integrated form of Eq. (19).

Because they introduce a correlation between the size of a step and its end point, neither the Stratonovich sum (22) nor the anti-Itô one (23) yield Eqs. (25) and (28)—just like Fick's law did not yield Eqs. (18) and (19) in Sec. III B. Instead, although this is less straightforward to show, only the anti-Itô formulation yields Fick's law, and therefore the moments associated to it [10,25,26] (Appendix B). The above discussion thus supports the use of Eq. (2), which corresponds to Itô diffusion, rather than Fick's law, to represent the diffusion of bouncing grains. The reason for this is that we can fairly represent the random walk of a bouncing grain as an explicit, unbiased process, wherein the noise manifests itself only when the grain hits the substrate, and vanishes while it is aloft.

The interpretation we propose thus departs from the conventional view that choosing the Itô, Stratonovich or anti-Itô formalism is just a matter of mathematical convenience, since an additional drift term turns one into the other. Instead, following Van Kampen [[25], p. 236] and Volpe and Wehr [10], we prefer to interpret these formulations as the continuous limits of distinct microscopic models that represent different physics. The drift term that distinguishes one from the other then takes on a physical meaning, and expresses itself visually in Chladni's experiment. From this perspective, bouncing grains are an instance of Itô diffusion, because the random impulse occurs at takeoff, and then fully determines the subsequent displacement.

This interpretation, hopefully, clarifies the debate between Tailleur and Cates [27], who concluded that Eq. (2) could not describe a random walk, and Schnitzer [28], who treated the same equation as a possible representation of heterogeneous diffusion. The first authors, indeed, used a continuous mechanism to represent random walks, in which the probability of moving or stopping was a function of the *current* particle position, thus excluding the possibility of Itô diffusion, wherein the particle carries the memory of its last jump over to the next bounce.

At this stage, it might be instructive to return to the conclusions of Sec. III B, and consider again the generality of Itô diffusion which, after the above, might appear as the unbiased—and therefore natural—generalization of homogeneous diffusion [29]. There is, however, no one-size-fits-all generalization. Brownian particles, for instance, are known to follow Fick's law, even when their diffusivity is heterogeneous [30]. If their motion is to be modeled with an overdamped random walk, therefore, it ought to be with the anti-Itô integral [10]—unlike bouncing grains. In other words, the Itô diffusion model presented here cannot represent Brownian particles in contact with a thermal bath, whose overdamped dynamics must relax to the Boltzmann distribution.

IV. HEAT FLUX

In the absence of any external force, bouncing grains gather in places of lesser diffusivity (Sec. III A), which are also colder places if Eq. (13) holds. While a statistical equilibrium can then be reached ($\mathbf{j} = 0$), it does not necessarily correspond to a thermodynamic equilibrium, wherein the heat flux $\mathbf{q}$ would vanish.

If, for illustration, we consider the heterogeneous substrate of Fig. 2(c), we can say that, at statistical equilibrium and per unit time, the number of particles entering the area corresponding to the soft pad equals that of the particles leaving it (on average). Now, those that exit carry, on average, more kinetic energy than those that enter, thus causing a heat flux from the soft pad to the rigid disk. In accordance with intuition, thus, the heterogeneity of the substrate induces a heat flux from hot places to colder ones.

Of course, this heat flux is a key component of the thermodynamics of bouncing grains. In particular, the leakage of heat along the temperature gradient of the BL motor is a fundamental limitation on the latter's efficiency [14], because it cannot be separated from the driving mechanism. We now use our experiments to assess the heat flux carried by bouncing grains in statistical equilibrium, when no horizontal force acts on them.

We now introduce a phenomenological model for the transport of horizontal kinetic energy—which we call heat. We assume that, during a jump, a grain typically carries the kinetic energy kT associated with its departure point. Combined with the particle flux law (2), this suggests

$$\mathbf{q} = -\nabla(D\rho kT), \tag{29}$$

where $\mathbf{q}$ is the heat flux parallel to the vibrating plate. This expression neglects possible correlations between the direction and the length of a jump, and the dissipation associated to flight and impact.

In statistical equilibrium, Eq. (3) implies that the heat flux becomes proportional to the temperature gradient:

$$\mathbf{q} = -k\langle\rho\rangle\langle D\rangle_h \nabla T, \tag{30}$$

where we have introduced $\langle\rho\rangle \equiv N/A$ to account for the total number of particles N, and the area A of the domain they explore. We may then define the thermal conductivity as $k\langle\rho\rangle\langle D\rangle_h$, which is a constant for a given system in statistical equilibrium. The system thus uniformizes its thermal conductivity as it relaxes toward steady state.

The temperature gradient in Eq. (30) becomes singular when the temperature field is discontinuous [14]. This is a problem in the present experiment, in which we assumed so far that the bouncing grains adjust their temperature instantly to local conditions. In reality, this adjustment most likely occurs over the course of a few bounces, that is, over a length of the order of the step size, which we write ℓ/γ, thus defining the dimensionless relaxation parameter γ. In statistical equilibrium, the total exchange of heat $\dot{\mathcal{Q}}$ through the boundary of the soft pad then reads

$$\dot{\mathcal{Q}} \approx k\langle\rho\rangle\langle D\rangle_h \frac{\gamma\Delta T}{\ell}\mathcal{L}, \tag{31}$$

where $\mathcal{L}$ is the length of the interface between the two types of substrates, and ΔT is the (macroscopic) temperature difference between the two corresponding domains. Combining Eqs. (6), (7), and (8), we can relate the step length to the temperature of a grain as

$$\ell = \frac{4kT\tan\theta}{mg}, \tag{32}$$

and thus rewrite the total heat flux (31) in a convenient form:

$$\dot{\mathcal{Q}} \approx \langle\rho\rangle\langle D\rangle_h \gamma \frac{mg\mathcal{L}}{4\tan\theta}\frac{\Delta T}{T}, \tag{33}$$

assuming that the relative change in temperature $\Delta T/T$ is not too large. Based on the grains' trajectories, we can measure every term in the above expression, and therefore estimate the value of the relaxation parameter γ.

For this, we need to evaluate the flux of kinetic energy through the boundary of the soft pad. We first collect all the segments in a trajectory that intersect the boundary of the soft pad, and record their direction s_i, as $s_i = 1$ (or $s_i = -1$) if the grains leaves (or enters) the soft pad. We first check that the mass balance is statistically in equilibrium, that is

$$\frac{1}{\sqrt{N_s}}\sum_{i=1}^{N} s_i \ll 1, \tag{34}$$

where N is the number of intersections for a single experimental movie. This ratio is 2×10^{-4} on average over all movies (and always less than 4×10^{-3}), indicating that our data set is large enough to estimate equilibrium statistics.

For each intersection, we also record the length of the trajectory segment that crosses the boundary. Since the frame rate of the camera is fixed, this gives us a (horizontal) crossing velocity v_i, based on which we estimate the heat flux as

$$\dot{\mathcal{Q}} = \frac{m}{2\tau_m}\sum_{i=1}^{N} s_i v_i^2 \tag{35}$$

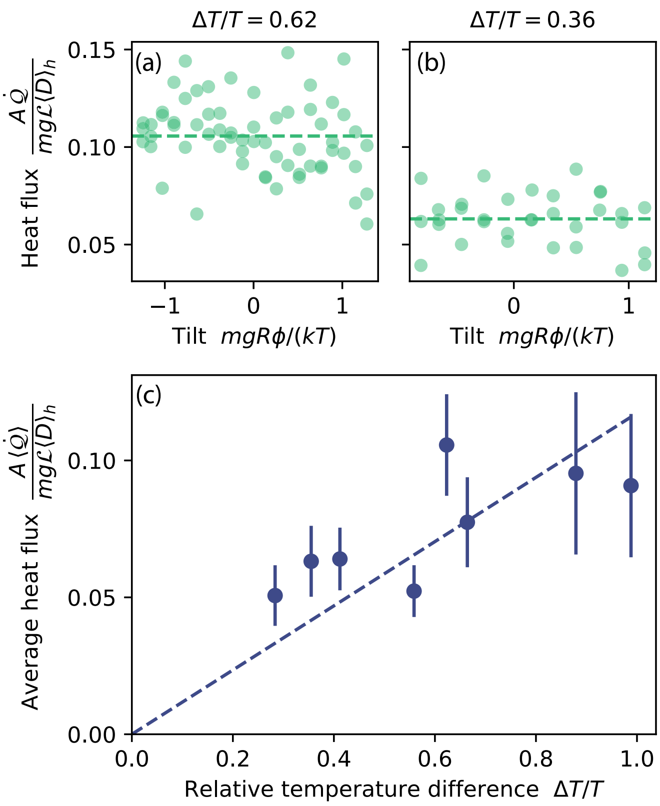

FIG. 9. Heat flux from the soft substrate to the hard substrate. (a), (b) Dimensionless heat flux for experiments A and B, respectively. Each dot corresponds to a movie. Dashed line: average value. (c) Average heat flux as a function of the relative temperature difference for experimental runs A to H. Dashed line: fitted linear relation with $\gamma = 1.75$, Eq. (33).

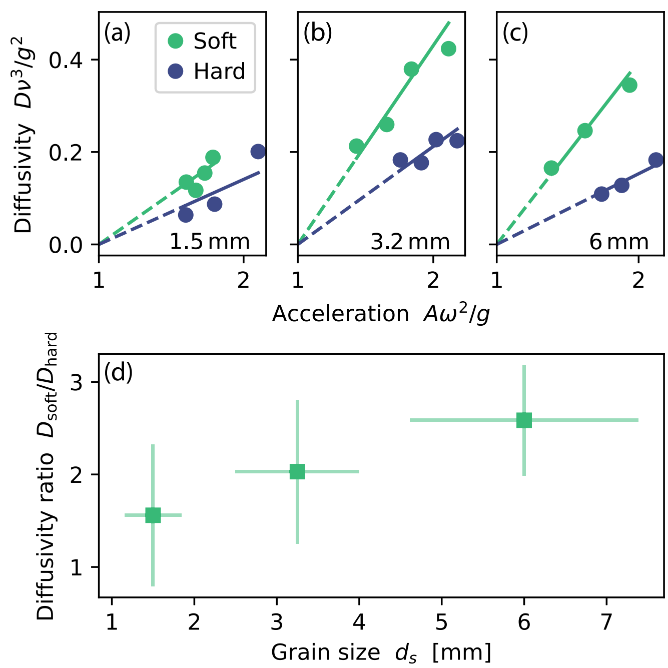

FIG. 10. Dependence of the grains' diffusivity on the vibration intensity. (a)–(c) Increase of diffusivity with dimensionless acceleration, for runs I and N (a), J and K (b), and L and M (c). Straight lines show proportional relation fitted to the data. (d) Dependence of the diffusivity ratio on grain size, based on the linear fit of panels (a)–(c).

for each experimental movie of duration τ_m. In Figs. 9(a) and 9(b), we represent this flux as a function of the tilt angle ϕ, which was varied for runs A to H. We find that, despite a large scatter, we can estimate a statistically significant heat flux. Its value does not seem to be much affected by the tilt of the setup in our experiment, probably because the temperature gradient is orthogonal to the force induced by the tilt. We thus use all the data we have to get better statistics, thus assuming we can neglect the external force when we measure the heat flux. Plotting the mean value of this flux as a function of the relative temperature difference, we find that our observations are compatible with a linear relation [Fig. 9(c)]. Fitting Eq. (33) to these data, we get an estimate of the relaxation parameter, $\gamma \approx 1.7 \pm 0.5$. As expected, its value is of order one.

V. DISCUSSION

In many respects, bouncing grains behave like Brownian particles. They diffuse like random walkers, and drift along external forces. Their temperature is well defined and they satisfy the fluctuation-dissipation relation. Their velocity also seems to follow the Maxwell-Boltzmann distribution. As long as their temperature is uniform, therefore, they can be treated as an analog of classical thermodynamics—perhaps a useful one in the classroom.

Before bringing this analog in front of students, however, one should keep in mind that this system departs from classical statistical physics in subtle ways. As soon as the diffusivity of the grains varies, indeed, their macroscopic behavior reveals the nature of their microscopic dynamics—a series of repeated, dissipating collisions with the vibrating plate.

This was visualized even before the establishment of statistical physics by Chladni [1], whose experiment shows the departure from Boltzmann's statistics in the form of convoluted nodal lines. To phrase it metaphorically, in Chladni's experiment, the grains carry their inertial memory forward in time, and forget all about it at the next bounce. Because the characteristics of each of their steps are fully determined at takeoff, their coarse-grained diffusion follows Eq. (2), which allows heterogeneous statistical equilibria that escape Fick's law. That the combination of path memory with its own erasure produces strange average dynamics should not surprise us—the bouncing droplets of Couder *et al.* [31] have been doing so for more than 20 years [32].

Due to the microscopic mechanism that draws them, Chladni figures are sustained at a cost. The vibrating substrate needs to supply the heat flux that necessarily arises from the heterogeneity of temperature. This flux follows a diffusion law that is consistent with Eq. (2)—at least, based on our observations. We interpret this disagreement with Fick's law as the macroscopic signature of an Itô random walk.

A remarkable property of the transport of heat by Itô diffusion is that, as the system reaches statistical equilibrium, its thermal conductivity becomes uniform, even though the density of grains does not, as shown by Eq. (30). This, again, would not be true with Fickian diffusion. Is this intriguing observation a coincidence, or does it reveal some deeper property of Itô diffusion? We would not venture any answer yet.

ACKNOWLEDGMENTS

The idea of the paper arose during seminal discussions with S. Protière. We are also grateful to E. Lajeunesse and F. Métivier for their help with the experiment, and to D. H. Rothman, G. Pucci, A. Eddi, W. Herreman, A. P. Petroff, A. Estevez-Torres, S. Djambov, A. J. C. Ladd and M. G. Worster for inspiring discussions. O.D. was partially funded by PhysErosion Grant No. ANR-22-CE30-0017.

DATA AVAILABILITY

The data that support the findings of this article are openly available [19].

APPENDIX A: ACCELERATION OF THE PLATE

Bouncing grains constantly dissipate energy, by friction with air and during their impact with the vibrating plate. The latter compensates for the energy loss by providing kinetic energy to the grains, in such a way as to maintain steady state. The mechanism by which this balance is reached is still unclear. It has attracted sustained attention in the simpler context of an elastic bead bouncing over a vibrating surface [33–35], due to its connection with the Feigenbaum cascade of bifurcations [36] and, ultimately, with the Fermi-Pasta-Ulam-Tsingou problem of thermalization [37]. Beyond a threshold acceleration ($A\omega^2/g$ large enough), such a bead bounces with an energy that increases with acceleration, perhaps linearly [38]. This is qualitatively consistent with the behavior of bouncing grains, whose diffusivity also increases with acceleration, although the specific expression of this dependency is not yet known [5].

We observe a similar behavior in the present experiment [Figs. 10(a)–10(c)]. For any grain size, diffusivity increases with the acceleration of the plate, and it is always larger over the soft substrate than over the hard one. Our data set does not allow us to make this observation systematic, but we can plot the ratio of the soft diffusivity to the hard one, to find that it increases with grain size [Fig. 10(d)]. We qualitatively interpret this observation as heavier grains being more sensitive to the softness of the elastomer—but we will not venture further than this speculation here. In this paper, we simply take its value as an experimental fact, which we use to interpret our observations.

APPENDIX B: FICKIAN DRIFT

Here we calculate the drift of a Fickian particle in a heterogeneous diffusivity field, following the procedure of Sec. III B. We again assume that the particle density and current vanish at infinity. We thus find

$$\begin{aligned}\frac{\partial\langle x\rangle}{\partial t} &= \int_{-\infty}^{\infty} x\,\frac{\partial}{\partial x}\left(D\frac{\partial\rho}{\partial x}\right)\mathrm{d}x\\ &= \int_{-\infty}^{\infty}\rho\,\frac{\partial D}{\partial x}\,\mathrm{d}x = \left\langle\frac{\partial D}{\partial x}\right\rangle\end{aligned}\tag{B1}$$

after integrating by parts twice. Unlike Eq. (2), Fick's law causes the mean position of a localized distribution to drift toward increasing diffusivity. As a result, to account for Fickian diffusion in the Itô representation, one needs to add a drift term proportional to the gradient of diffusivity. On average, therefore, a Brownian particle moves toward places of higher diffusivity. This remark shows that, when diffusivity is heterogeneous, Fick's law represents a biased random walk.

In the same fashion, we can now compute the spread of a parcel of Brownian particles in a heterogeneous diffusivity field, according to Fick's law:

$$\begin{aligned}\frac{\partial\langle x^2\rangle}{\partial t} &= \int_{-\infty}^{\infty} x^2\,\frac{\partial}{\partial x}\left(D\frac{\partial\rho}{\partial x}\right)\mathrm{d}x\\ &= 2\langle D\rangle + 2\left\langle x\frac{\partial D}{\partial x}\right\rangle.\end{aligned}\tag{B2}$$

This result is similar to Eq. (19), but for an additional contribution proportional to the diffusivity gradient.

[1] E. F. F. Chladni, *Entdeckungen über die Theorie des Klanges* (Bey Weidmanns Erben Und Reich, Leipzig, 1787).

[2] M. Faraday, On a peculiar class of acoustical figures; and on certain forms assumed by groups of particles upon vibrating elastic surfaces, Philos. Trans. R. Soc. London **121**, 299 (1831).

[3] A. Kudrolli, G. Lumay, D. Volfson, and L. S. Tsimring, Swarming and swirling in self-propelled polar granular rods, Phys. Rev. Lett. **100**, 058001 (2008).

[4] J. Arango and C. Reyes, Stochastic models for Chladni figures, Proc. Edinburgh Math. Soc. **59**, 287 (2016).

[5] A. Abramian, S. Protière, A. Lazarus, and O. Devauchelle, Chladni patterns explained by the space-dependent diffusion of bouncing grains, Phys. Rev. Res. **7**, L032001 (2025).

[6] I. Grabec, Vibration driven random walk in a Chladni experiment, Phys. Lett. A **381**, 59 (2017).

[7] M. Büttiker, Transport as a consequence of state-dependent diffusion, Z. Phys. B **68**, 161 (1987).

[8] R. Landauer, Motion out of noisy states, J. Stat. Phys. **53**, 233 (1988).

[9] N. Van Kampen, Relative stability in nonuniform temperature, IBM J. Res. Dev. **32**, 107 (1988).

[10] G. Volpe and J. Wehr, Effective drifts in dynamical systems with multiplicative noise: A review of recent progress, Rep. Prog. Phys. **79**, 053901 (2016).

[11] A. Raja Venkatesh, K. H. Le, D. M. Weld, and O. Brandman, Diffusive lensing as a mechanism of intracellular transport and compartmentalization, eLife **12**, RP89794 (2024).

[12] O. Devauchelle, P. Popović, P. Szymczak, A. Abramian, and A. Lazarus, companion paper, Granular Büttiker-Landauer motor, Phys. Rev. Lett. **137**, 097101 (2026).

[13] F. Berger, T. Schmiedl, and U. Seifert, Optimal potentials for temperature ratchets, Phys. Rev. E **79**, 031118 (2009).

[14] R. Benjamin and R. Kawai, Inertial effects in Büttiker-Landauer motor and refrigerator at the overdamped limit, Phys. Rev. E **77**, 051132 (2008).

[15] gPhoto^2 digital-camera Unix software, http://gphoto.org/.

[16] Munkres (Hungarian) algorithm for the assignment problem in Python, https://pypi.org/project/munkres/.

[17] S. van der Walt, J. L. Schönberger, J. Nunez-Iglesias, F. Boulogne, J. D. Warner, N. Yager, E. Gouillart, T. Yu, and the scikit-image contributors, Scikit-image: Image processing in Python, PeerJ **2**, e453 (2014), https://scikit-image.org/.

[18] BrownTrack Python library, https://github.com/odevauchelle/BrownTrack/tree/main.

[19] O. Devauchelle, P. Popovic, P. Szymczak, A. Lazarus, and A. Abramian, Thermodynamics of bouncing grains and Büttiker-Landauer motor [Data set], Zenodo, https://zenodo.org/records/18862698.

[20] H. Risken, *The Fokker-Planck Equation Methods of Solution and Applications*, 2nd ed. (Springer, Berlin, 1989).

[21] P. F. Tupper and X. Yang, A paradox of state-dependent diffusion and how to resolve it, Proc. Royal Soc. A Math. Phys. Eng. Sci. **468**, 3864 (2012)

[22] S. Giordano and R. Blossey, Effective diffusion constant of stochastic processes with spatially periodic noise, Phys. Rev. E **110**, 044123 (2024).

[23] P. Hänggi, Nonlinear fluctuations: The problem of deterministic limit and reconstruction of stochastic dynamics, Phys. Rev. A **25**, 1130 (1982).

[24] Stratonovich and anti-Itô integrals are nonetheless the overdamped limit of different classes of dynamics [10,25].

[25] N. G. Van Kampen, *Stochastic Processes in Physics and Chemistry* (Elsevier, Amsterdam, 1992), Vol. 1.

[26] E. Wong and M. Zakai, On the convergence of ordinary integrals to stochastic integrals, Ann. Math. Stat. **36**, 1560 (1965).

[27] J. Tailleur and M. E. Cates, Statistical mechanics of interacting run-and-tumble bacteria, Phys. Rev. Lett. **100**, 218103 (2008).

[28] M. J. Schnitzer, Theory of continuum random walks and application to chemotaxis, Phys. Rev. E **48**, 2553 (1993).

[29] This discussion owes much to A. P. Petroff (personal communication).

[30] L. P. Faucheux and A. J. Libchaber, Confined Brownian motion, Phys. Rev. E **49**, 5158 (1994).

[31] Y. Couder, S. Protière, E. Fort, and A. Boudaoud, Walking and orbiting droplets, Nature (London) **437**, 208 (2005).

[32] E. Fort, A. Eddi, A. Boudaoud, J. Moukhtar, and Y. Couder, Path-memory induced quantization of classical orbits, Proc. Natl. Acad. Sci. USA **107**, 17515 (2010).

[33] P. Pierański, Jumping particle model. Period doubling cascade in an experimental system, J. Physique **44**, 573 (1983).

[34] S. Warr, W. Cooke, R. Ball, and J. Huntley, Probability distribution functions for a single-particle vibrating in one dimension: Experimental study and theoretical analysis, Physica A **231**, 551 (1996).

[35] J.-Y. Chastaing, E. Bertin, and J.-C. Géminard, Dynamics of a bouncing ball, Am. J. Phys. **83**, 518 (2015).

[36] A. Lichtenberg, M. Lieberman, and R. Cohen, Fermi acceleration revisited, Physica D **1**, 291 (1980).

[37] S. Ulam, On some statistical properties of dynamical systems, in *Proceedings of the 4th Berkeley Symposium on Mathematical Statististics and Probability* (University of California Press, Berkeley and Los Angeles, 1961), Vol. 3, pp. 315–320.

[38] J.-C. Géminard and C. Laroche, Energy of a single bead bouncing on a vibrating plate: Experiments and numerical simulations, Phys. Rev. E **68**, 031305 (2003).